Electronic Supplementary Material (ESI) for Journal of Materials Chemistry

Supporting Information

Dye Metachromasy on Titanate Nanowires: Sensing Humidity with Reversible Molecular Dimerization

By *Endre Horváth*, Primož Rebernik Ribič, Fatemeh Hashemi, László Forró, Arnaud Magrez**

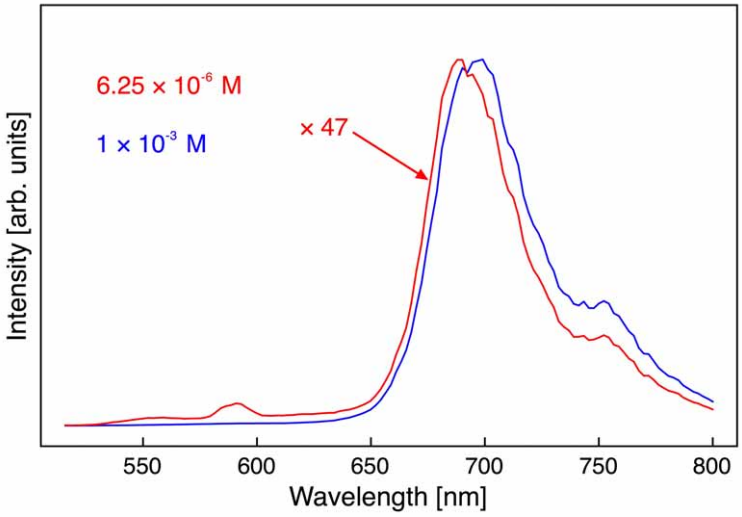

Figure S1 Laser induced fluorescence spectra of concentrated (1×10^{-3} molL^{-1}) (blue) and dilute (6.25×10^{-6} molL^{-1}) (red) solutions of MB in water

Further experiments were performed in order to obtain more insight into the aggregation process of MB. Figure S1 shows laser induced fluorescence spectra of concentrated (1×10^{-3} molL^{-1}) and dilute (6.25×10^{-6} molL^{-1}) solutions of MB in water. An excitation wavelength of 488 nm was chosen, because at this wavelength the molar absorption coefficient only very weakly depends on the MB concentration [1,2]. Although the ratio of the concentrations is 160, the fluorescence peak (at around 690 nm) intensity ratio is only around 47. This is a clear indication that the fluorescence is substantially quenched

in the case of the concentrated solution. Dimerization related concentration quenching of fluorescence in dye solutions is a well-known and well-documented phenomenon [see, e.g., Ref. [3] and references therein]. Assuming that dimerization is the only aggregation process of MB in water, one can calculate the monomer concentrations for the two solutions according to Ref. [4]. In our case we get a monomer concentration of 3.0×10^{-4} $molL^{-1}$ for the concentrated solution and 6.0×10^{-6} $molL^{-1}$ for the dilute solution, yielding a monomer concentration ratio of 50. This factor is in good agreement with the fluorescence intensity peak ratio and suggests that the fluorescence signal comes mainly from the MB monomers in the solution. Dimerization of MB in the concentrated solution is also confirmed by a small redshift (from 691 nm to 697 nm) of the fluorescence peak [5].

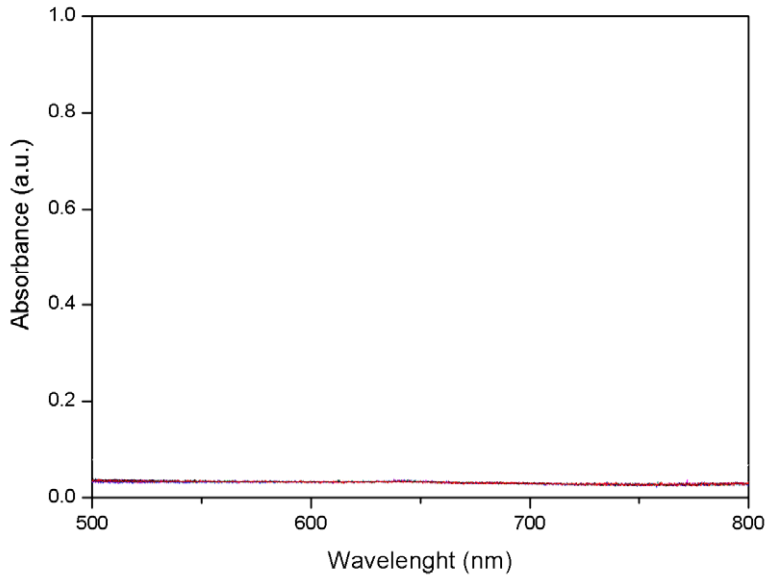

Figure S2 UV-Vis spectrum (recorded over 15h) of supernatant solution for testing MB

desorption in water. The spectrum is representative of spectrum recorded with other solvents including organic ones. The absence of MB signal confirms the irreversible adsorption of MB on titanate nanowires.

Calibration for the Relative Humidity Sensor

The calibration method is based upon the use of saturated salt solutions as the humidity generation source. Saturated salt solutions were placed in a sealed container. The relative humidity above the salt depends slightly on the temperature. A list of saturated salts and their humidity values at 25°C are shown in the table below.

Table 1.

Material	**Silica gel**	**KOH**	**$Mg(NO_3)_2.6H_2O$**	**NH_4Cl**	**$CuSO_4*5H_2O$**
RH (%)	0	8	52	77	98

In order to minimize the transient time the the air volume per unit area of the solution surface was less than 15 cm^3:1 cm^{-2}. The sensor was placed into a low-volume (3 cm^3) test enclosure connected to the jar containing the wet salt with a hermetic seal (**Fig. S3**). The circulation of the air was driven with a peristaltic pump (flux of 1.6 cm^3s^{-1}). Before the read-out the air circulation was continued for 1 hour for the air inside the sensor to reach the steady relative humidity level.

Calculation of the MB surface density

After reaching the MB adsorption equilibrium the MB adsorption capacity on titanate nanowires was found to be 86 mg/g. If we assume that the molecules are uniformly distributed on the nanowire surface, and taking into account that the specific surface area

was 160 m^2/g, the number of the adsorbed MB molecules can be calculated with the following equation:

$$SMB \approx \frac{aMB * NA}{M(MB) * SA(TiONW)}$$

where aMB is the maximum MB adsorption capacity, NA is the Avogadro number, M(MB) is the molar mass of MB and SA(TiONW) is the specific surface area of the titanate nanowires calculated from nitrogen adsorption-desorption measurements [6].

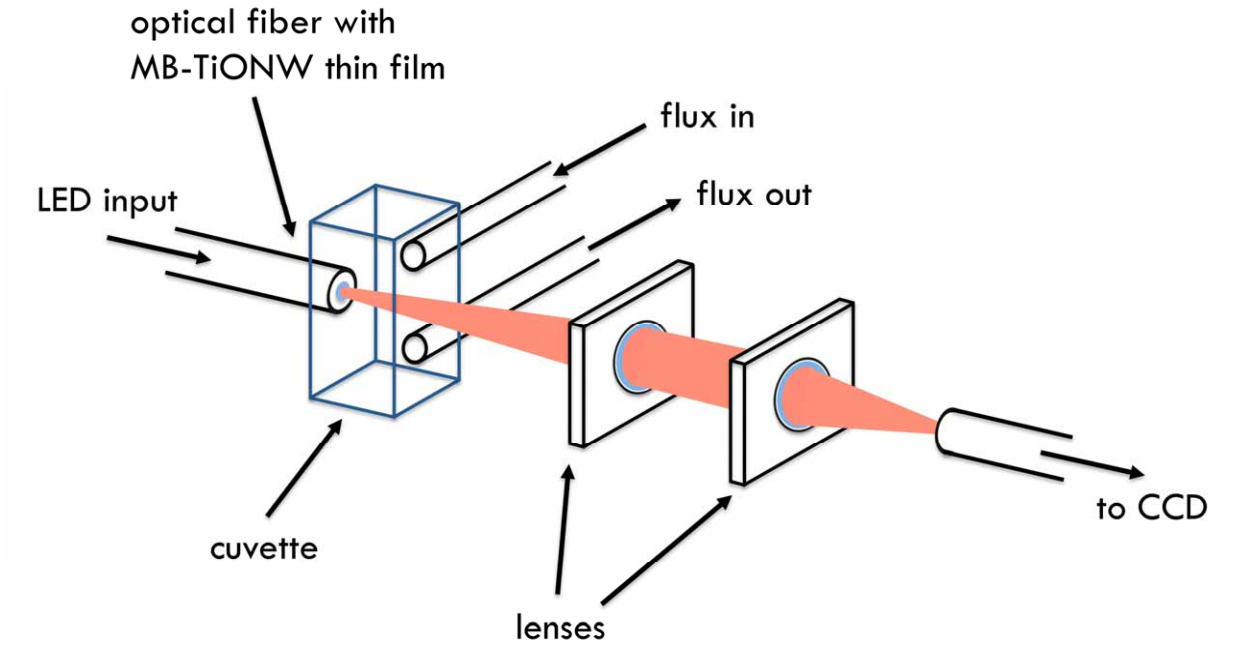

Figure S3. The scheme of the experimental setup for the sensor measurements

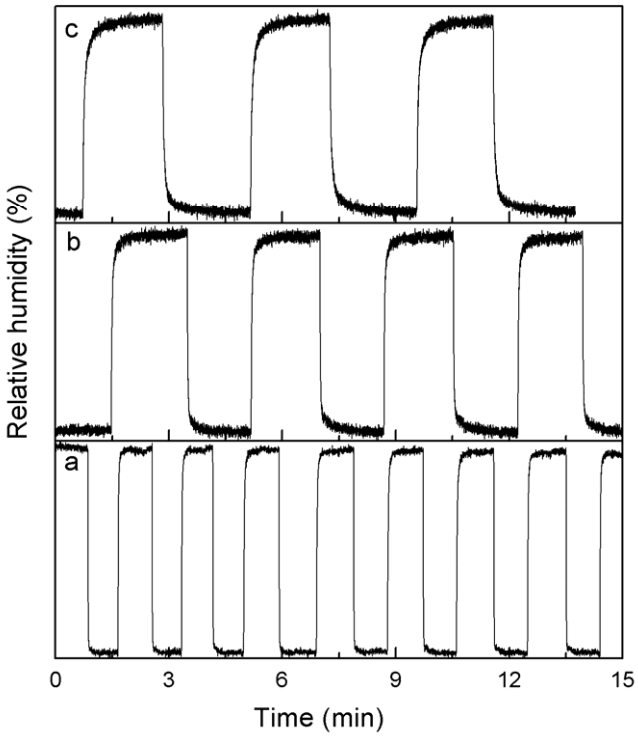

Figure S4 Multiple response and recovery cycles for the MB-TiONW thin film when relative humidity changes from high (98 %) to low (8 %) levels. The measurements were performed at a wavelength of 650 nm using different air fluxes: (a) 30 cm^3s^{-1}, (b) 16.4 cm^3s^{-1} (c) 6.8 cm^3s^{-1}

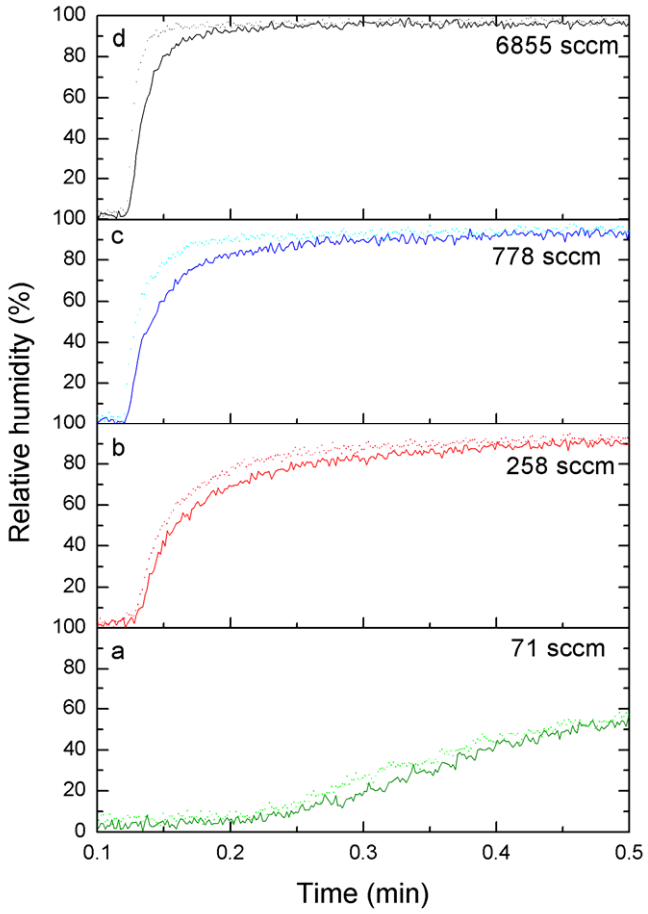

Figure S5. MB@TiONW humidity sensor's representative response (dotted line) and the reciprocal recovery signals (continuous line) vs. gas flux. (a) 1.6 cm^3s^{-1}, (b) 6.8 cm^3s^{-1}, (c) 16.4 cm^3s^{-1}, (d) 30 cm^3s^{-1}

In order to measure the response of the OFHS due to humidification and desiccation the sensor is placed in a chamber that is connected with a peristaltic pump. (See **Fig. S3.**) To calculate the velocity of the air stream flowing trough the sensor, the flux coming from the peristaltic pump was corrected for the volume of the tubing system entering into the measuring chamber. (**Fig. 4g**) Note that the highest flux used (30 cm^3s^{-1}) only matches

the lowest 0 category on the modern Beaufort Wind Force Scale. Some of the sensors we have fabricated for this study lasted for more than few weeks without modification of their performances. Further studies are necessary to assess the stability over years.

Table 2.

Sensing properties of some optical humidity sensors

Materials (cladding)	Measuring principle (form)	Usable linear range (RH%)	Response-recovery time	Ref.
$CoCl_2$/cellulose	Optical (film)	4-60 %	16-60 min	[7]
NiO	Optical (film)	0-90 %	≤3 min	[8]
Dye/zeolite	Optical (disk)	9-92 %	2-4 min	[9]
Dye/polymer,(F1/PMMA)	Optical (fiber)	8-85 %	1 s	[10]
$CoCl_2$/gelatin	Optical (fiber)	0-40 %, 40-70 %, 70-100 %	≈1 s	[11]
Silica xerogel	Optical (fiber)	44-100 %	10 -120 s	[12]
Au/polymer	Optical (fiber)	11-100 %	< 1.5 s	[13]
Co/polyaniline	Optical (fiber)	20-95 %	8-60 s	[14]
Hydroxyethylcellulose	Optical (fiber)	40-70 %	3-10 s	[15]
Rhodamine B/ hydroxypropyl cellulose	Optical (fiber)	0-95 %	60- 180 s	[16]
Agarose gel	Optical (fiber)	30-80 %	< 60 s	[17]

[1] E. Rabinowitch, L. F. Epstein, *J. Am. Chem. Soc.* **1941**, *63*, 69.

[2] K. Bergmann, C. T. O'Konski, *J. Phys. Chem.* **1963**, *67*, 2169.

[3] K. K. Rohatgi, G. S. Singhal, *J. Phys. Chem.* **1966**, *70***,** 1695.

[4] A. Mills, J. Wang, *J. Photoch. Photobio. A* **1999**, *127*, 123.

[5] R. R. Naujok, R. V. Duevel, R. M. Corn, *Langmuir* **1993**, *9*, 1771.

[6] E. Horváth, Á. Kukovecz, Z. Kónya, I. Kiricsi, *Chem. Mater.*, **2007**, *19*, 927.

[7] F. Boltinghouse, A. Kenneth, *Anal. Chem.* **1989**, *61*, 1863.

[8] M. Ando, J. Sato, S. Tamura, T. Kobayashi, *Solid State Ionics* **1999**, *121*, 307.

[9] S. Sohrabnezhad, A. Pourahmad, M. A. Sadjadi, *Materials Letters* **2007**, *61*, 2311.

[10] S. Muto, H. Sato, T.Hosaka, *Jpn. J. Appl. Phys.* **1994**, *33*, 6060.

[11] A. Kharaz, B.E.Jones, *Sensors and Actuators* A **1995**, *46-47*, 491.

[12] J. Estella, P. de Vincente, J. C. Echeverría, J. J. Garrido, *Sensors and Actuators* B **2010**, *149*, 122.

[13] F. J. Arregui, Y. Liu, I. R. Matias, R. O. Claus, *Sensors and Actuators* B **1999**, *59*, 54.

[14] A. Vijayan, M. Fuke, R. Hawaldar, M. Kulkarni, D. Amelnelkar, R.C. Aiyer, *Sensors and Actuators* B **2008**, *129*, 106.

[15] S. Muto, O. Suzuki, T. Amano, M. Morosawa, *Meas. Sci. Technol*. **2003**, *14*, 746.

[16] S. Otsuki, K. Adachi, T. Taguchi, *Sensors and Actuators* B **1998**, *53*, 91.

[17] C. Bariáin, I. R. Matías, F. J. Arregui, M. López-Amo, *Sensors and Actuators* B **2000**, *69*, 127.

[18] N. Tétreault, E. Horváth, T. Moehl, J. Brillet, R. Smajda, S. Bungener, N. Cai, P. Wang, P. S. M. Zakeeruddin,; L. Forró, A. Magrez, M. Grätzel, *ACS Nano* **2010**, *4*, 7644.